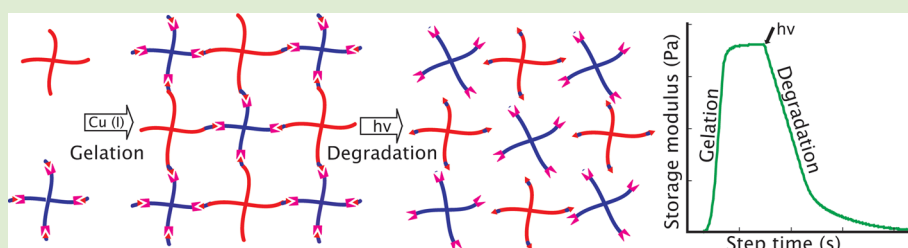


# Coumarin-Based Photodegradable Hydrogel: Design, Synthesis, Gelation, and Degradation Kinetics

Malar A. Azagarsamy,<sup>||,†,‡,§</sup> Daniel D. McKinnon,<sup>||,†,§</sup> Daniel L. Alge,<sup>†,‡,§</sup> and Kristi S. Anseth<sup>\*,†,‡,§</sup>

<sup>†</sup>Department of Chemical and Biological Engineering, <sup>‡</sup>BioFrontiers Institute, and <sup>§</sup>Howard Hughes Medical Institute, University of Colorado, Boulder, Colorado 80303, United States

## Supporting Information



**ABSTRACT:** The design, synthesis, and characterization of a new class of coumarin-based photodegradable hydrogels are reported. Hydrogel formation was achieved rapidly and efficiently under aqueous conditions using copper-catalyzed click chemistry, which afforded excellent control over the rate of network formation. Rapid photodegradation, to the point of reverse gelation, was observed using both 365 and 405 nm light, and micrometer-scale features were eroded using two-photon irradiation at wavelengths as long as 860 nm.

Hydrogels, water-swollen cross-linked polymeric networks, are an important class of polymeric materials in biomedical research. For applications in tissue engineering and regenerative medicine, some of the key properties of hydrogels are their ability to localize and deliver therapeutic proteins in a controlled manner, serve as delivery vehicles for cell transplantation, and allow the culture of stem cells in tissue-like three-dimensional microenvironments *in vitro*.<sup>1–3</sup> Degradable hydrogels are among the most attractive and useful classes of hydrogel scaffolds, as their degradability can be leveraged to control the release and delivery of therapeutic cells and proteins.<sup>4–7</sup> Conventionally, hydrogel degradation is achieved either hydrolytically or proteolytically; these approaches to degradability are often mediated by internal triggers such as pH, temperature, small molecules, and enzymes.<sup>8–11</sup> However, there is a growing interest among researchers in developing chemical strategies that externally allow for spatiotemporal control over the cleavage of gel cross-links.<sup>2,12–14</sup> To this end, photodegradable hydrogels, which allow for precise user-directed degradation of the network structure via light-mediated reactions, have evolved and received enormous attention in recent years.<sup>15–17</sup> While these hydrogels have been found to have numerous applications to date,<sup>18–21</sup> the majority of the systems reported are based on incorporating a photolabile nitrobenzyl moiety into the network cross-links.<sup>15,16,22</sup>

In this letter, we introduce a coumarin-based photodegradable hydrogel platform as a potential alternative to the previously reported nitrobenzyl-based systems. Importantly, this chemistry is highly suitable for biological applications, as the photodegradation reaction produces biologically inert

byproducts.<sup>23,24</sup> Unlike the nitrobenzyl system, which releases an aldehyde or ketone, both of which are reactive toward amine functionalities of proteins,<sup>25,26</sup> the coumarin system exposes a less reactive alcohol.<sup>23,24,27,28</sup> An additional advantage of this coumarin-based platform is the red shift in its degradation wavelengths, which provides access to a broader spectrum of cytocompatible wavelengths of light.<sup>23,24,27,28</sup> Here, the synthesis of a new class of coumarin-based hydrogels, which are cross-linked using aqueous copper-catalyzed click chemistry,<sup>29–32</sup> is described. In addition, characterization of the gel formation and photodegradation properties of these hydrogels is presented.

The macromolecular precursors 4-armed poly(ethylene glycol) (PEG) tetra-alkyne **1** and 4-armed PEG tetracoumarin azide **2** used in the formation of the photodegradable hydrogels are shown in Figure 1. Polymer **1** was synthesized in a straightforward manner upon reacting 4-armed 5 kDa PEG tetra-amine with pentynoic acid. The coumarin-based polymeric precursor **2** was obtained by coupling 4-armed 5 kDa PEG tetracarboxylic acid with an amine-terminated coumarin azide **3**. This coumarin azide **3** was synthesized following the synthetic route described in Scheme 1. Briefly, 7-amino-methylcoumarin was first diazotized and then treated with sodium azide to obtain 7-azido-methylcoumarin **4**. The methyl functionality of the coumarin was then oxidized to a methylene alcohol using selenium dioxide as an oxidizing agent. The

Received: April 15, 2014

Accepted: May 14, 2014

Published: May 16, 2014



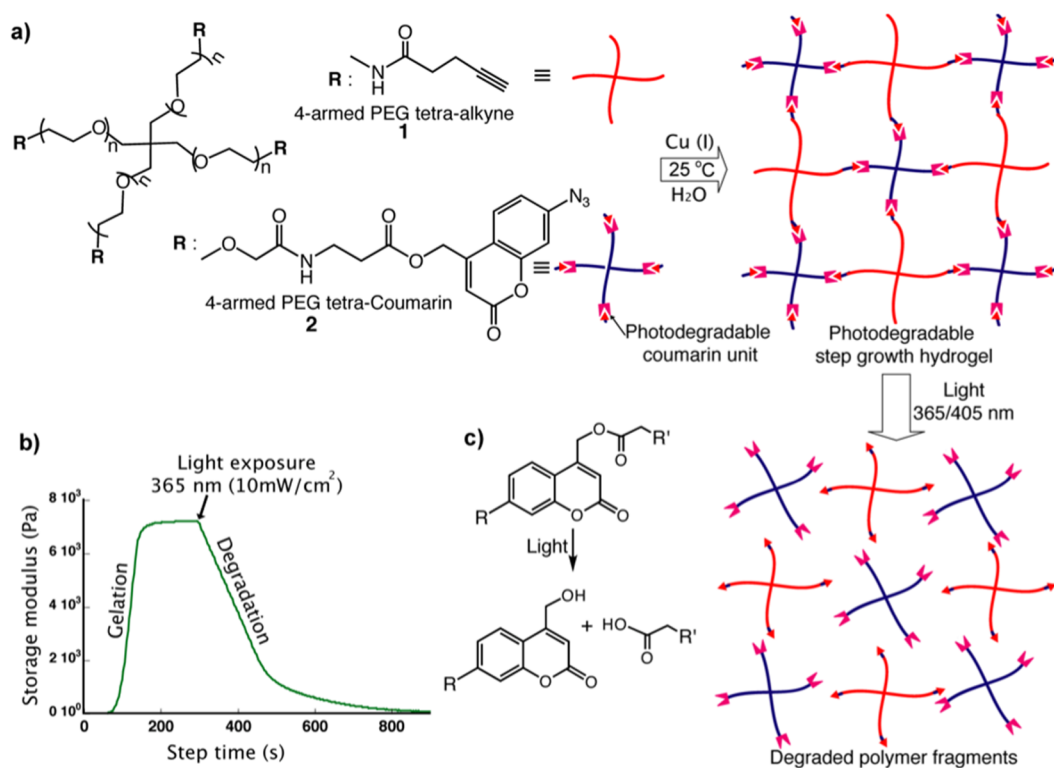
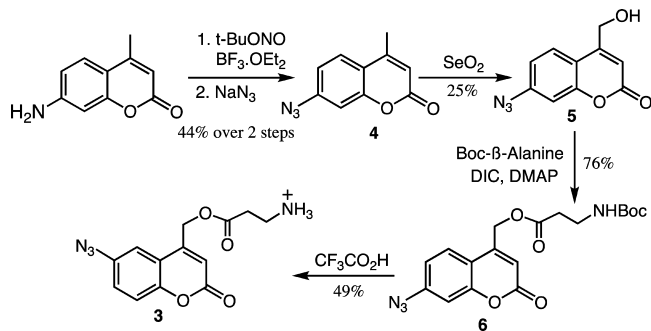


**Figure 1.** Coumarin-based photodegradable hydrogel: (a) Chemical structures of 4-arm PEG tetra-alkyne (5 kDa) and 4-arm PEG tetra-azide (5 kDa) and schematic representation of copper(I)-catalyzed gel formation and light-activated degradation. (b) In situ rheology of gelation and degradation of coumarin hydrogels. Gelation and degradation were achieved at 2–16 mM of Cu(I) and at 365 nm (10 mW/cm<sup>2</sup>) of light, respectively, under aqueous conditions at room temperature. (c) Photochemistry of coumarin methyl ester degradation, in which coumarin methyl alcohol is produced after degradation.

### Scheme 1. Synthesis of Amine-Terminated Coumarin Azide 3



resultant coumarin methyl alcohol 5 was then coupled to Boc-protected beta-alanine and exposed to trifluoroacetic acid to obtain the final amine-containing coumarin azide 3.

Hydrogel formation was achieved by mixing equimolar (100 mg/mL, 80 mM functional groups) aqueous solutions of 1 and 2 with solutions of sodium ascorbate (316 mg/mL, 1.6 M), followed by copper sulfate at varying concentrations (Figure 1). The final concentrations of alkyne and azide functional groups were 36 mM, and the final concentration of sodium ascorbate was 80 mM. The concentration of copper sulfate was varied from 2 to 16 mM to investigate the effects of this variable on the gelation characteristics, specifically the kinetics of gel formation and the final modulus reached during in situ polymerization on a shear rheometer. As expected, a correlation between the concentration of copper sulfate and the gelation kinetics was observed, where higher concentrations resulted in

faster network formation (Figure 2A). For example, with 0.44 equiv of copper per alkyne (16 mM), the modulus reached 90% of the final value within 2 min, while reducing the copper concentration to 0.05 equiv (2 mM) delayed this conversion to over 15 min. In general, the time required to reach 90% of the final modulus (based on when the macromers were placed on the rheometer) varied over an order of magnitude from ca. 100 s to ca. 1000 s. To quantify the kinetics of gel formation, we measured the time elapsed between the gel point and the gel reaching 90% of its final modulus to avoid errors associated with the time required to initiate measurements (Figure 2B and Table SI 1, Supporting Information). These times were inverted to generate rates of modulus evolution, which varied linearly with respect to copper concentration (Figure SI 1, Supporting Information). This analysis indicates that the copper is involved in the rate-limiting step, and the rate of modulus evolution corresponds well with the rate of the click reaction, which is also linear with respect to copper concentration.<sup>31–33</sup>

Interestingly, the copper sulfate concentration also had an effect on the modulus of the final hydrogel, as higher catalyst concentrations resulted in lower final moduli (Figure 2A, C). For example, decreasing the copper concentration from 0.44 to 0.05 equiv per alkyne nearly doubled the final modulus achieved. Previous reports on building polymers using click reactions have shown no change in conversion with respect to the copper concentration. Thus, the effect of copper concentration on final modulus is likely driven by the kinetics of gel formation, leading to different network structures and nonidealities.<sup>31</sup> While the opposite trend was previously observed for thermally initiated thiol–ene step growth gels,<sup>34</sup>

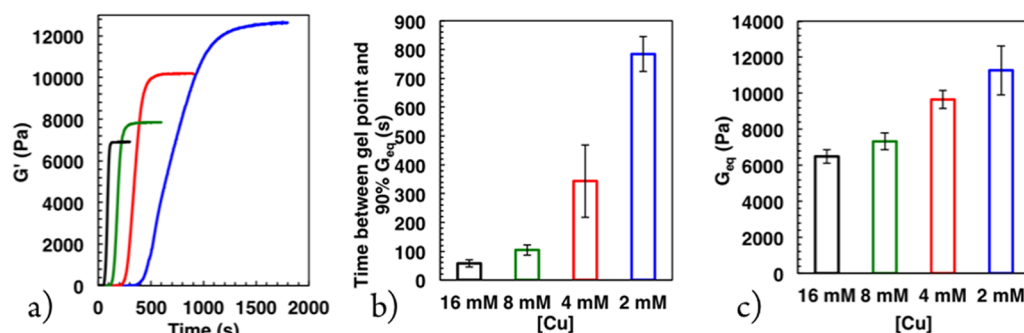


**Figure 2.** Coumarin-based photodegradable hydrogel formation kinetics: (a) In situ copper(I)-catalyzed gel formation at various concentrations of copper. The concentration of copper sulfate was 16 mM for black, 8 mM for green, 4 mM for red, and 2 mM for blue. (b) Time to reach 90% of the final modulus from the gel point with varying copper concentrations. (c) Mean equilibrium shear elastic modulus achieved by gels polymerized using different concentrations of copper.

we hypothesize that the more complicated mechanism of triazole formation may be responsible for this difference. With this cross-linking chemistry, three collisions are necessary to achieve bond formation: (i) copper(II) and sodium ascorbate to form copper(I), (ii) copper(I) and alkyne to form the activated copper(I)/alkyne complex, and (iii) the copper(I)/alkyne complex and azide for cross-link formation.<sup>33</sup> Consequently, rapid gelation may potentially restrict functional group mobility and lead to network nonidealities (e.g., loops or unreacted end groups), which would likely reduce the cross-link density and modulus. Work is ongoing to elucidate a potential mechanism for the reaction rate dependent modulus observation.

After characterizing the network formation in these step growth hydrogels, detailed characterization of the photodegradation reaction was performed. Previous work has demonstrated that the coumarin moiety cleaves in response to UV (365 nm) and visible (405 nm) light at vastly different rates. Bone morphogenetic proteins (BMPs) tethered to a hydrogel network through a coumarin linker were shown to be released 3.3 times faster than those tethered through a nitrobenzyl linker under 365 nm irradiation and 2.9 times slower under 405 nm irradiation at the same light intensity.<sup>28</sup> We sought to investigate and quantify the rates of coumarin cleavage upon exposure to different intensities of 365 and 405 nm light through hydrogel degradation kinetic studies. Coumarin cross-linked hydrogels were polymerized in situ and exposed to varying intensities of both 365 and 405 nm light. We observed significant differences in the time required for cross-link cleavage, as measured by modulus reduction, over the range of intensities and wavelengths investigated. The shear elastic modulus of coumarin cross-linked hydrogels exposed to 1.4 mW/cm<sup>2</sup> of 405 nm irradiation was reduced to only ca. 95% of its initial value after 200 s, while hydrogels exposed to 10.4 mW/cm<sup>2</sup> 365 nm experienced a modulus reduction to less than 25% of its initial value at the same time point (Figure 3A,B and Table SI 2, Supporting Information). This behavior was fit to a first-order degradation model shown in eq 1 to yield apparent rates of cross-linking cleavage that can be quantified and compared.<sup>15,16</sup>

$$G(t) = G_0 e^{-k_{app} t} \quad (1)$$

Here,  $G$  is the shear elastic modulus;  $G_0$  is the initial shear elastic modulus; and  $t$  is the time of exposure. The apparent rate of degradation,  $k_{app}$ , has been shown to depend on the quantum yield,  $\phi$ , the molar absorptivity,  $\epsilon$ , the incident

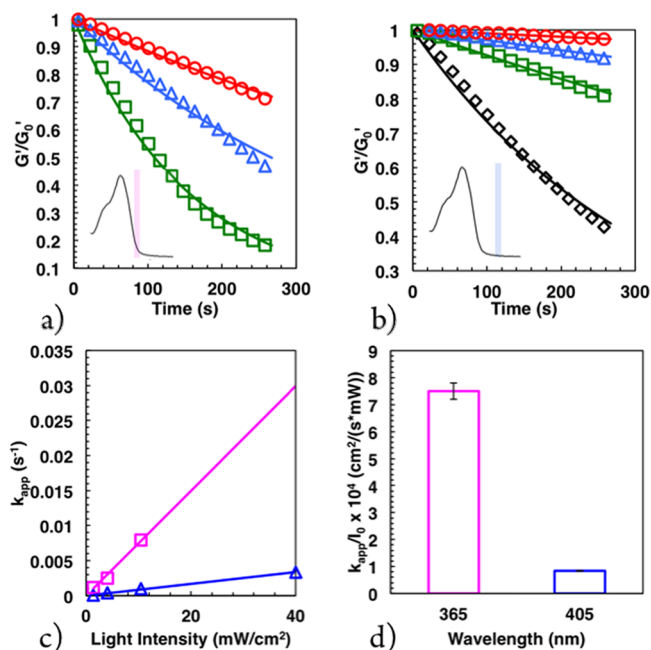


**Figure 3.** Coumarin-based photodegradable hydrogel degradation kinetics: (a) In situ rheology of the coumarin gel degrading in response to 365 nm light. The data are shown as points, and the fit is shown as a line. Green is 10.4 mW/cm<sup>2</sup>, blue is 4.0 mW/cm<sup>2</sup>, and red is 1.4 mW/cm<sup>2</sup>. The absorbance of the material along with a band representing 365 nm is shown in the inset. (b) In situ rheology of the coumarin gel degrading in response to 405 nm light. Black is 40 mW/cm<sup>2</sup>, green is 10.4 mW/cm<sup>2</sup>, blue is 4.0 mW/cm<sup>2</sup>, and red is 1.4 mW/cm<sup>2</sup>. The absorbance of the material along with a band representing 405 nm is shown in the inset. (c) Plot of  $k_{app}$  versus light intensity. Across a wavelength, a straight line is expected with data (points) and fits (lines) shown for 365 nm (magenta) and 405 nm (violet). Error bars are smaller than the points. (d)  $k_{app}/I_0$  versus light intensity. Both these numbers collapse to  $k_{app}/(I_0 \epsilon) \times 10^4 = 0.0030 \pm 0.0001$  cm<sup>3</sup> M/(s mW) when normalized to the extinction coefficient,  $\epsilon$ , of the material at those wavelengths.

irradiation,  $I_0$ , and the wavelength of light,  $\lambda$ . This relationship is shown in eq 2, where  $N_A$  is Avogadro's number,  $h$  is Planck's constant, and  $c$  is the speed of light. Thus, the rate of gel degradation can be modulated by changing light intensity or wavelength, as the molar absorptivity is a function of wavelength.<sup>15,16</sup>

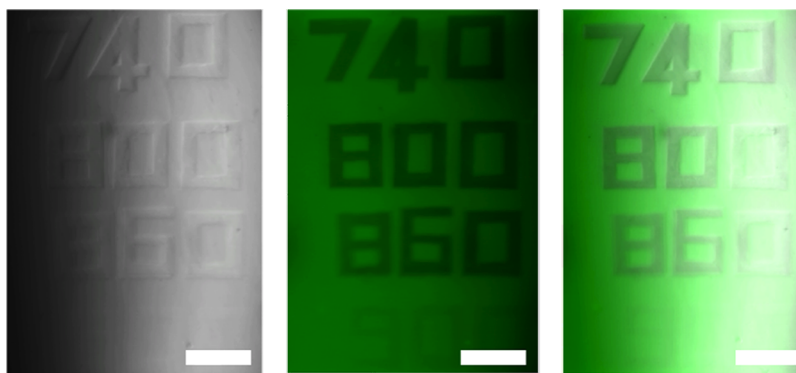


**Figure 4.** Images of two-photon degradation. The coumarin gel is fluorescent in response to 405 nm incident light. Thus, transmitted, fluorescent, and merged images are shown (left, center, and right, respectively). The numbers refer to the two-photon wavelength used to degrade the material. Degradation and gel erosion were tested up to 900 nm of two-photon light. However, degradation at 900 nm was inefficient. Scale bar: 100  $\mu\text{m}$ .

$$k_{\text{app}} = \frac{\phi \epsilon \lambda I_0 (2.303 \times 10^{-6})}{N_A h c} \quad (2)$$

The shear elastic modulus of coumarin cross-linked hydrogels was monitored during exposure to 40, 10.4, 4.0, and 1.4  $\text{mW}/\text{cm}^2$  of 405 nm light and 10.4, 4.0, and 1.4  $\text{mW}/\text{cm}^2$  of 365 nm light. The resulting data were plotted and fit to eq 1 (Figure 3). The apparent rate constant,  $k_{\text{app}}$ , varied by almost 2 orders of magnitude, from  $1.0 \times 10^{-4} \text{ s}^{-1}$  under exposure to 1.4  $\text{mW}/\text{cm}^2$  405 nm light to  $79 \times 10^{-4} \text{ s}^{-1}$  under 10.4  $\text{mW}/\text{cm}^2$  365 nm light. Because the degradation is a first-order process, the rates of degradation at each wavelength are expected to collapse to a single point when normalized for light intensity (Figure 3 and Tables S2 and S3, Supporting Information). In general, we observed excellent agreement with this theory and show consistent  $k_{\text{app}}/I_0$  for a given wavelength. Furthermore, based on these calculations, the coumarin cross-linked gel degraded with 365 nm light at a rate comparable to the fastest nitrobenzyl moieties reported.<sup>16</sup> While the degradation kinetics were roughly ten times slower at 405 nm, this result is consistent with the absorbance data showing that the PEG-coumarin molecule 2 absorbs slightly less than ten times more light at 365 nm ( $\epsilon = 2460 \text{ cm}^{-1} \text{ M}^{-1}$  per functional group) than at 405 nm ( $\epsilon = 280 \text{ cm}^{-1} \text{ M}^{-1}$  per functional group). When this difference in molar absorptivity is taken into account, all of the data collapse to a single value,  $k_{\text{app}}/(I_0 \epsilon) \times 10^4 = 0.0030 \pm 0.0001 \text{ cm}^3 \text{ M}/(\text{s mW})$ , indicating that the quantum yield is similar for both wavelengths of light.

Finally, we hypothesized that the coumarin moiety would also cleave in response to longer wavelengths of two-photon light. Using a confocal microscope and a tunable two-photon laser, we observed visible material degradation for wavelengths between 720 and 860 nm (Figure 4). While the efficiency of degradation was much higher at 740 nm, requiring only a 1.58  $\mu\text{s}$  pixel dwell at a 110  $\text{mW}/\mu\text{m}^2$  intensity, degradation was observed even out to 860 nm by increasing the pixel dwell time.

In conclusion, our results demonstrate the utility of coumarin-based photodegradable moieties for user-directed manipulation of hydrogel materials. Importantly, this chemistry is efficient at longer wavelengths of light and produces biologically benign byproducts upon photocleavage. Although this characterization has been performed using hydrogels cross-linked by copper-catalyzed click chemistry, this coumarin chemistry could easily be adapted to a cytocompatible copper-free hydrogel platform.<sup>13,28,35–39</sup> Thus, we anticipate that this versatile new chemistry will prove useful in future tissue

engineering studies focused on spatiotemporal patterning of cellular microenvironments.

## ■ ASSOCIATED CONTENT

### 📄 Supporting Information

Raw absorbance data, tables of raw kinetic values, and additional experimental methods. This material is available free of charge via the Internet at <http://pubs.acs.org>.

## ■ AUTHOR INFORMATION

### ✉ Corresponding Author

\*E-mail: [kristi.anseth@colorado.edu](mailto:kristi.anseth@colorado.edu).

### ✍ Author Contributions

<sup>||</sup>M.A.A. and D.D.M. contributed equally. The manuscript was written through contributions of all authors. All authors have given approval to the final version of the manuscript.

### 📄 Notes

The authors declare no competing financial interest.

## ■ ACKNOWLEDGMENTS

Funding from the National Science Foundation (CBET 1236662) and the Howard Hughes Medical Institute. The authors acknowledge Tobin Brown for helpful discussions regarding the manuscript.

## ■ REFERENCES

- (1) Slaughter, B. V.; Khurshid, S. S.; Fisher, O. Z.; Khademhosseini, A.; Peppas, N. A. *Adv. Mater.* **2009**, *21*, 3307–3329.
- (2) Azagarsamy, M. A.; Anseth, K. S. *ACS Macro Lett.* **2012**, *2*, 5–9.
- (3) McKinnon, D. D.; Kloxin, A. M.; Anseth, K. S. *Biomater. Sci.* **2013**, *1*, 460–469.
- (4) Gumbley, P.; Koyle, D.; Pawle, R. H.; Umezuruike, B.; Spedden, E.; Staii, C.; Thomas, S. W., III. *Chem. Mater.* **2014**, *26*, 1450–1456.
- (5) Bryant, S. J.; Anseth, K. S. *J. Biomed. Mater. Res.* **2001**, *59*, 63–72.
- (6) Fairbanks, B. D.; Schwartz, M. P.; Halevi, A. E.; Nuttelman, C. R.; Bowman, C. N.; Anseth, K. S. *Adv. Mater.* **2009**, *21*, 5005–5010.
- (7) Lutolf, M. P.; Hubbell, J. A. *Biomacromolecules* **2003**, *4*, 713–722.
- (8) McKinnon, D. D.; Domaille, D. W.; Cha, J. N.; Anseth, K. S. *Chem. Mater.* **2014**, *26*, 2382–2387.
- (9) Zhang, Z.-X.; Liu, K. L.; Li, J. *Angew. Chem., Int. Ed.* **2013**, *52*, 6180–6184.
- (10) Ehrbar, M.; Schoenmakers, R.; Christen, E. H.; Fussenegger, M.; Weber, W. *Nat. Mater.* **2008**, *7*, 800–804.
- (11) Lutolf, M. P.; Lauer-Fields, J. L.; Schmoekel, H. G.; Metters, A. T.; Weber, F. E.; Fields, G. B.; Hubbell, J. A. *Proc. Natl. Acad. Sci.* **2003**, *100*, 5413–5418.
- (12) Patterson, J.; Hubbell, J. A. *Biomaterials* **2010**, *31*, 7836–7845.

- (13) McKinnon, D. D.; Domaille, D. W.; Cha, J. N.; Anseth, K. S. *Adv. Mater.* **2013**, *26*, 865–872.
- (14) Lee, K. Y.; Bouhadir, K. H.; Mooney, D. J. *Biomaterials* **2004**, *25*, 2461–2466.
- (15) Kloxin, A. M.; Kasko, A. M.; Salinas, C. N.; Anseth, K. S. *Science* **2009**, *324*, 59–63.
- (16) Griffin, D. R.; Kasko, A. M. *J. Am. Chem. Soc.* **2012**, *134*, 13103–13107.
- (17) Wong, D. Y.; Griffin, D. R.; Reed, J.; Kasko, A. M. *Macromolecules* **2010**, *43*, 2824–2831.
- (18) Kloxin, A. M.; Benton, J. A.; Anseth, K. S. *Biomaterials* **2010**, *31*, 1–8.
- (19) Wang, H.; Haeger, S. M.; Kloxin, A. M.; Leinwand, L. A.; Anseth, K. S. *PLoS One* **2012**, *7*, e39969.
- (20) Wang, H.; Tibbitt, M. W.; Langer, S. J.; Leinwand, L. A.; Anseth, K. S. *Proc. Natl. Acad. Sci.* **2013**, *110*, 19336–19341.
- (21) Azagarsamy, M. A.; Alge, D. L.; Radhakrishnan, S. J.; Tibbitt, M. W.; Anseth, K. S. *Biomacromolecules* **2012**, *13*, 2219–2224.
- (22) Ercole, F.; Thissen, H.; Tsang, K.; Evans, R. A.; Forsy, J. S. *Macromolecules* **2012**, *45*, 8387–8400.
- (23) Babin, J.; Pelletier, M.; Lepage, M.; Allard, J.-F.; Morris, D.; Zhao, Y. *Angew. Chem., Int. Ed.* **2009**, *48*, 3329–3332.
- (24) Zhao, Y.; Zheng, Q.; Dakin, K.; Xu, K.; Martinez, M. L.; Li, W.-H. *J. Am. Chem. Soc.* **2004**, *126*, 4653–4663.
- (25) Givens, R. S.; Rubina, M.; Wirz, J. *Photochem. Photobiol. Sci.* **2012**, *11*, 472–488.
- (26) Du, X.; Frei, H.; Kim, S.-H. *Biopolymers* **2001**, *62*, 147–149.
- (27) Furuta, T.; Wang, S. S. H.; Dantzker, J. L.; Dore, T. M.; Bybee, W. J.; Callaway, E. M.; Denk, W.; Tsien, R. Y. *Proc. Natl. Acad. Sci.* **1999**, *96*, 1193–1200.
- (28) Azagarsamy, M. A.; Anseth, K. S. *Angew. Chem., Int. Ed.* **2013**, *52*, 13803–13807.
- (29) Malkoch, M.; Vestberg, R.; Gupta, N.; Mespouille, L.; Dubois, P.; Mason, A. F.; Hedrick, J. L.; Liao, Q.; Frank, C. W.; Kingsbury, K.; Hawker, C. J. *Chem. Commun.* **2006**, 2774–2776.
- (30) Spruell, J. M.; Wolffs, M.; Leibfarth, F. A.; Stahl, B. C.; Heo, J.; Connal, L. A.; Hu, J.; Hawker, C. J. *J. Am. Chem. Soc.* **2011**, *133*, 16698–16706.
- (31) Binauld, S.; Boisson, F.; Hamaide, T.; Pascault, J. P.; Drockenmuller, E.; Fleury, E. *J. Polym. Sci. A, Polym. Chem.* **2008**, *46*, 5506–5517.
- (32) Bock, V. D.; Hiemstra, H. *Eur. J. Org. Chem.* **2006**, 51–68.
- (33) Rostovtsev, V.; Green, L.; Fokin, V.; Sharpless, K. B. *Angew. Chem., Int. Ed.* **2002**, *41*, 2596–2599.
- (34) Cook, W. D.; Chen, F.; Pattison, D. W.; Hopson, P.; Beaujon, M. *Polymer* **2007**, *56*, 1572–1579.
- (35) Alge, D. L.; Azagarsamy, M. A.; Donohue, D. F.; Anseth, K. S. *Biomacromolecules* **2013**, *14*, 949–953.
- (36) Grover, G. N.; Lam, J.; Nguyen, T. H.; Segura, T.; Maynard, H. D. *Biomacromolecules* **2012**, *13*, 3013–3017.
- (37) Zheng, J.; Smith Callahan, L. A.; Hao, J.; Guo, K.; Wesdemiotis, C.; Weiss, R. A.; Becker, M. L. *ACS Macro Lett.* **2012**, *1*, 1071–1073.
- (38) Truong, V. X.; Ablett, M. P.; Gilbert, H.; Bowen, J.; Richardson, S. M.; Hoyland, J. A.; Dove, A. P. *Biomater. Sci.* **2014**, *2*, 167–175.
- (39) Fan, Y.; Deng, C.; Cheng, R.; Meng, F.; Zhong, Z. *Biomacromolecules* **2013**, *14*, 2814–2821.